Journal of Mechanics in Medicine and Biology
Vol. 22, No. 4 (2022) 2230001 (28 pages)

DOI: 10.1142/S0219519422300010

World Scientific
www.worldscientific.com

FINITE ELEMENT SPINE MODELS AND SPINAL INSTRUMENTS: A REVIEW

SALIHA ZEYNEB AKINCI*,‡ and YUNUS ZIYA ARSLAN†,§

*Department of Biomedical Engineering and Bioinformatics
Graduate School of Engineering and Natural Sciences
Istanbul Medipol University, 34810 Beykoz, Istanbul, Turkey

†Department of Robotics and Intelligent Systems
Institute of Graduate Studies in Science and Engineering
Turkish-German University, Beykoz, Istanbul 34820, Turkey
‡szakinci@medipol.edu.tr
§yunus.arslan@tau.edu.tr

Received 2 November 2021
Accepted 4 February 2022
Published 22 April 2022

There is considerable biomechanics literature on finite element modeling and analysis of the spine. To accurately mimic the biomechanical behavior of the vertebral column, a generated computational model has to include anatomical structures that are consistent with physiological reality. In this review article, we focused on the finite element spine models that have been developed by various approaches in the literature. Firstly, the anatomical features of the spine and the spinal components have been briefly explained. We then focused on the modeling stages of vertebrae, ligaments, facet joints, intervertebral discs, and spinal instruments. With this paper, we expect to provide a comprehensive resource regarding the modeling preferences used in spine modeling.

Keywords: Finite element method; spine models; reconstruction of imaging data; biomechanical behavior.

1. Introduction

The spine is a dynamic structure made up of vertebrae, intervertebral discs, and soft tissues (muscles, nerves, spinal cord, and ligaments). From the biomechanical point of view, the spine plays a crucial role in the transmission of dynamic loads and moments resulting from the head, trunk, and pelvis movements. A healthy spine functions properly with strong bones and muscles, flexible tendons, ligaments, and nerves. It is a complex and flexible system that is allowing individuals to stand

‡Corresponding author.

upright, bend and twist, protecting the spinal cord from injury within the neuromuscular control system.[1,2]

Among all other medical conditions, spinal disorders have taken a vital place in the health-related quality of life. Spinal surgery is a developing area in today's clinical medicine as a therapeutic measure.[2] Technological advances have significant implications for modern spinal disorder treatments. The main goal of pharmaceutical, biological, and mechanical treatments is to relieve back pain. However, there are not so many technological alternatives for the treatment of spine disease.[3] Decompression and fusion are the main treatment for intractable back pain, which involves the employment of bone grafts, metal plates, metal rods, and screws.[3]

Scoliosis is a sideways curvature of the spine associated with the degeneration of spinal components such as the intervertebral disc, facet joint, and vertebral bone.[4,5] Also, osteoporosis is another reason for degeneration to some extent.[5,6] The degeneration of the intervertebral discs and facet joints causes the spinal column to misalign in the coronal plane.[5,7] Surgical interventions are performed on the spine with severe or progressive deformities.[8–11] Determination of the spinal muscle forces or stresses across the vertebrae and intervertebral discs would provide valuable insight regarding the postoperative outcomes of the surgeries. Several studies have been conducted to measure *in vivo* spinal muscle forces and intervertebral loads by using some experimental techniques.[12,13] However, since these techniques are highly invasive and ethically questionable, only a few studies experimentally determined the spinal loads and muscle forces in living people.[14–16] At this point, computational biomechanical models and simulations are considered as an alternative for the noninvasive determination of muscle and spinal loads.[6,8,17,18]

As a result of the development of computational methods, and because of the flexibility in representation of the biomechanical features of the soft and hard tissues and less ethical concerns, finite element (FE) models have gained popularity and have been used as a practical alternative for *in vivo* and *in vitro* testing methods.[12,19–21] However, due to the unique biomechanical features of the spine, it is challenging to develop physiologically reliable and accurate FE spine models.[10] Therefore, verification, validation, and calibration of FE model simulations should be critically conducted before making clinical implications.[6,8,22]

In this review paper, after briefly addressing the spine structure, we evaluated FE spine models developed with various approaches in the literature. We also introduced and discussed the modeling stages of the vertebrae, ligaments, facet joints, and intervertebral discs with an emphasis on the scoliotic spine and spinal implants.

2. Anatomical Structure of the Spine

The vertebral column (spine or backbone) is constituted of several parts like bones, joints, tendons, and muscles extending from the skull to the pelvis. It is a complex and flexible system allowing individuals to stand upright, bend, and twist and also protect the spinal cord from injury.[1,2]

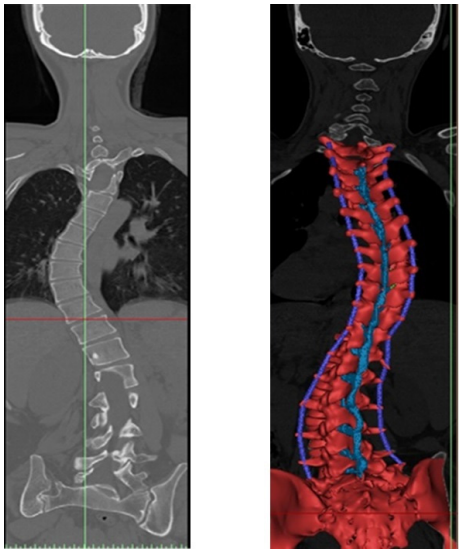

Fig. 1. (Color online) CT image showing the spinal curvature of a scoliotic patient and the three-dimensional model of the spinal components in different colors (vertebrae, discs, facet joints (in red color), and ligaments (in blue and purple colors)).

The computed tomography (CT) image of a patient with scoliosis is seen in Fig. 1. Compared to a healthy spine, the scoliotic spine has an abnormal curvature that describes the deformity, especially in the thoracic region.

The thoracic spine is the most common location for the scoliotic curve and it has significant importance in several ways.[23] The thoracic spine and the ribs protect the lungs and the heart, and also this region has a role in the reflection of the sympathetic afferent flow in the nervous system through the other organs. As a result of dysfunctions in this region, lesions can be seen as a mobility loss. Biomechanical influences of these lesions can be seen in the vertebrae, joints, and other structures of the thoracic region.[1,24,25]

If there is a structural deformity in the frontal plane, then scoliosis leads to lateral curvature of the spine and rotation of the vertebrae. The diagnosis of this disorder can be performed by physical examination and imaging techniques like X-rays, CT, or magnetic resonance imaging (MRI) scans. Scoliosis can be treated with orthopedic interventions depending on the condition of the curvature of the spinal column.[1,2,25]

To maintain the correct alignment of the spine, the applied loads on the spine should be delivered equally with the help of spinal instrumentation. The diseased portion of the spine can be stabilized by using spinal instrumentation and this mechanical system can distribute loading over the spinal components. Additionally, spinal implants can be more effective with appropriate mechanical characteristics like high material strength, toughness, and fatigue resistance.[2] The construction of

the spinal implants should have a basis involving these special features and the total loading should be transferred through the vertebral column during flexion and extension, torsional loading, and side bending.

To analyze the biomechanics of the spine function, load–displacement characteristics of the corresponding region should be evaluated in the functional spinal unit, which represents the central biomechanics and functional characteristics of the entire spine.[25–27]

2.1. *Structure of the vertebrae*

In different regions of the spine (cervical, thoracic, or lumbar spine), structural differences of the vertebrae can be seen, but generally, they look similar. Each of them consists of a body, an arch, and various processes (Fig. 2). The structural differences between the different vertebrae can be detected in Fig. 3. Figure 3(a) indicates the thoracic vertebrae from the second level to the last of this region (from T2 to T12). The anatomical structures of the whole lumbar vertebrae (from L1 to L5, Fig. 3(b)) are slightly different from those of the thoracic region. The lumbar vertebrae are larger and heavier than vertebral bodies in other regions.

2.2. *Structure of the intervertebral disc*

The intervertebral disc is the main load-bearing structure in a healthy spine.[28] This complex structure resists and absorbs various loads and experiences large deformations through the vertebral column and provides the flexibility of the spine.[29]

The intervertebral disc is composed of water, collagen, proteoglycans, and other matrix proteins and consists of an inner gelatinous core, the nucleus pulposus, a surrounding ring, the annulus fibrosus, and the cartilaginous endplates.[29] The three-dimensional (3D) full intervertebral disc structure and the corresponding neighboring segments of this spinal region are shown in Fig. 4.

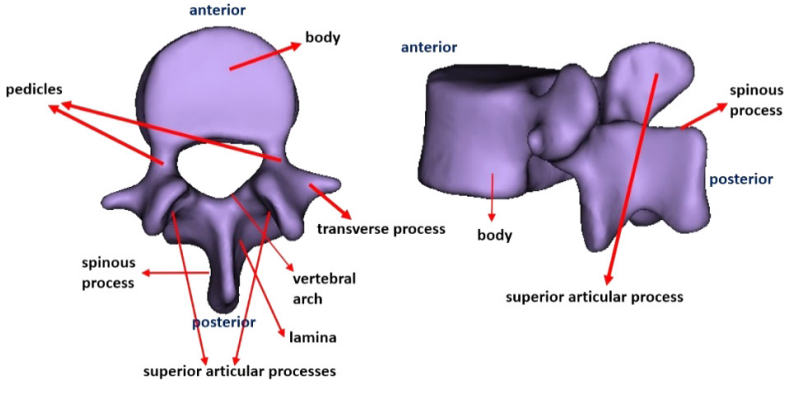

Fig. 2. General structure of a vertebra.

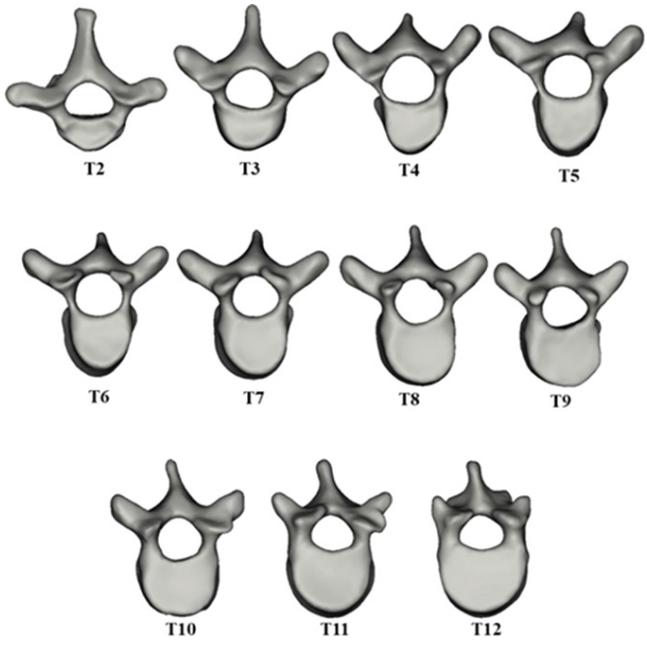

(a)

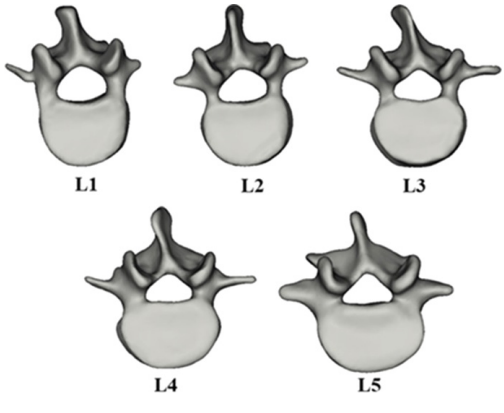

(b)

Fig. 3. Representation of the (a) thoracic vertebrae (T2–T12) and (b) lumbar vertebrae (L1–L5).

2.3. *Structure of the facet joints*

The facet joint has complicated anatomical and morphological features as well as mechanical characteristics that affect the whole behavior of the vertebral column. Facet joints exist in pairs at each spinal level on the posterior parts of the lateral segments of each vertebra. Figure 5 indicates the region of two facet joints after the segmentation process is completed.

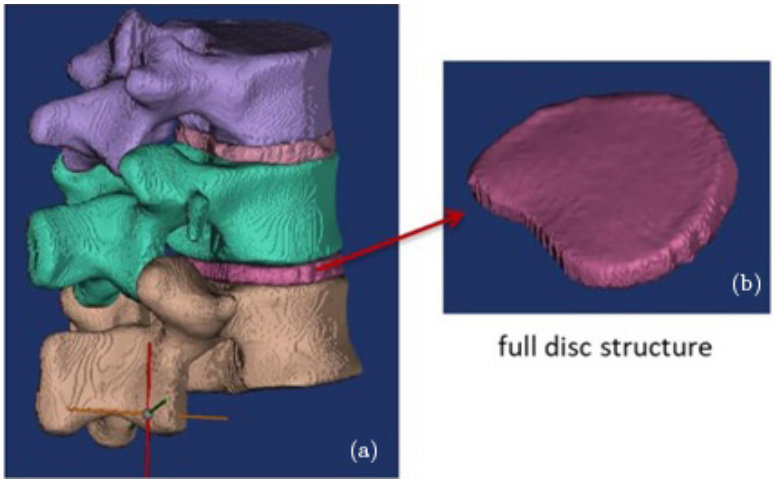

Fig. 4. (a) 3D model of the vertebrae and intervertebral discs and (b) full disc structure between the neighboring segments of this model.

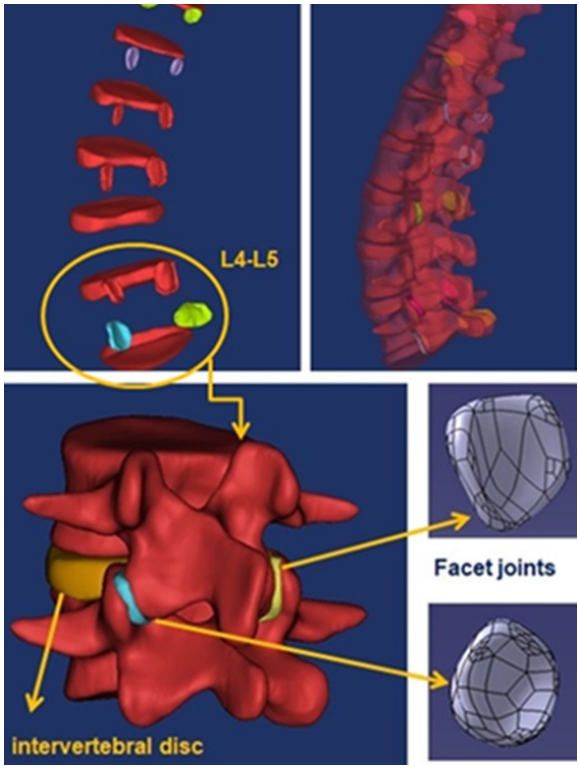

Fig. 5. Anatomical orientation of a facet joint between two vertebrae.

In a healthy human spine, there is a low-friction interface between the cartilage surfaces of the facet joint that facilitates the motion. The anatomical features, orientation, and mechanical behavior affect the spine response against external loading as a result of the interaction with intervertebral discs.[30]

The orientation of the facet joints is different in specific parts of the spine and it alters in different people as well. While the facet joints are vertically located in the thoracic region, the ones in the lumbar region are approximately oriented as parallel to the upper direction.[28]

2.4. *Structure of the ligaments*

From the clinical perspective, it is vital to preserve the functionality and stability of the spinal column in the case of structural disorders of the spine.[31] Ligaments are important spinal constituents that keep the stability of the spine.[32] These spinal components, which are strong fibrous tissues, hold the spinal column together and protect the intervertebral discs by stabilizing the applied loads.[1,33]

There are three major ligaments in the spine. These are the ligamentum flavum, anterior longitudinal ligament, and posterior longitudinal ligament (Fig. 6). In addition to providing stability, they have an important role in limiting the spinal column from excessive movement.[31] Additionally, the anterior and posterior ligaments beginning from the top of the vertebral column to the end of the sacrum prevent excessive motions of the spine. The third major ligament, the ligamentum flavum, exists as an attachment between the spinous processes of the vertebral column.[1,33]

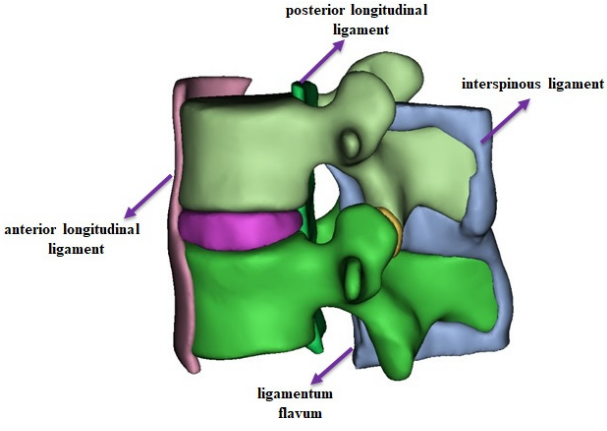

(a)

Fig. 6. Major ligaments (ligamentum flavum, anterior and posterior longitudinal ligaments) in the vertebral column of (a) L2–L3 and (b) T10–sacrum.

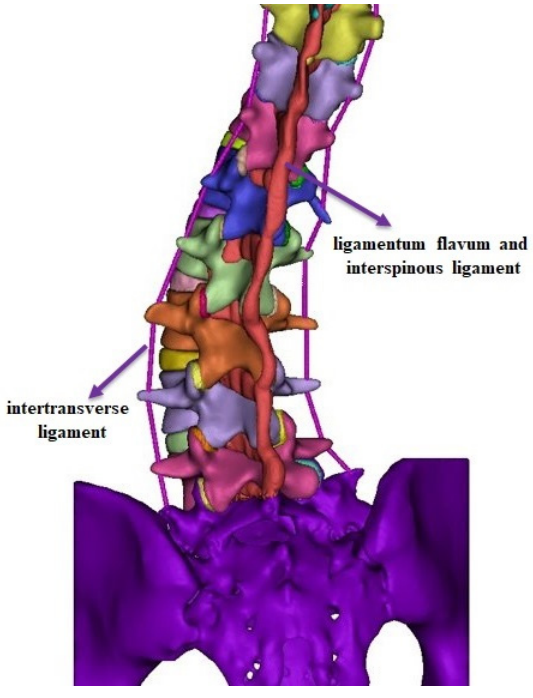

(b)

Fig. 6. (*Continued*)

3. Digitization of the Spine Anatomy: Segmentation and Construction of the 3D Model of the Spine

CT is a two-dimensional imaging technique that can be used to diagnose or detect spinal column damage in injured patients. The CT scan images have been also employed in the construction of the 3D model of the spinal structures that can be simulated in the FE analysis. The working principle of CT is based on the measurement of the tissue absorption/attenuation coefficient of radiation, which is relatively quantified with the Hounsfield unit (HU) and can be related to bone density. Different densities of the bone allow separating the cancellous and cortical layers of the bone.[34]

The FE modeling of the musculoskeletal system has several steps including image segmentation, reconstruction, mesh generation, mesh optimization, and assignment of material properties.[35]

There are various techniques for determining accurate geometries of the spinal structures.[36] CT scans of living and cadaver human specimens have been used to obtain the geometry of the spine models.[22,36–39] In the development of a model from a CT data set, there are several steps to be taken (Fig. 7). First of all, surface extraction from the CT scan should be performed for obtaining the geometry of the

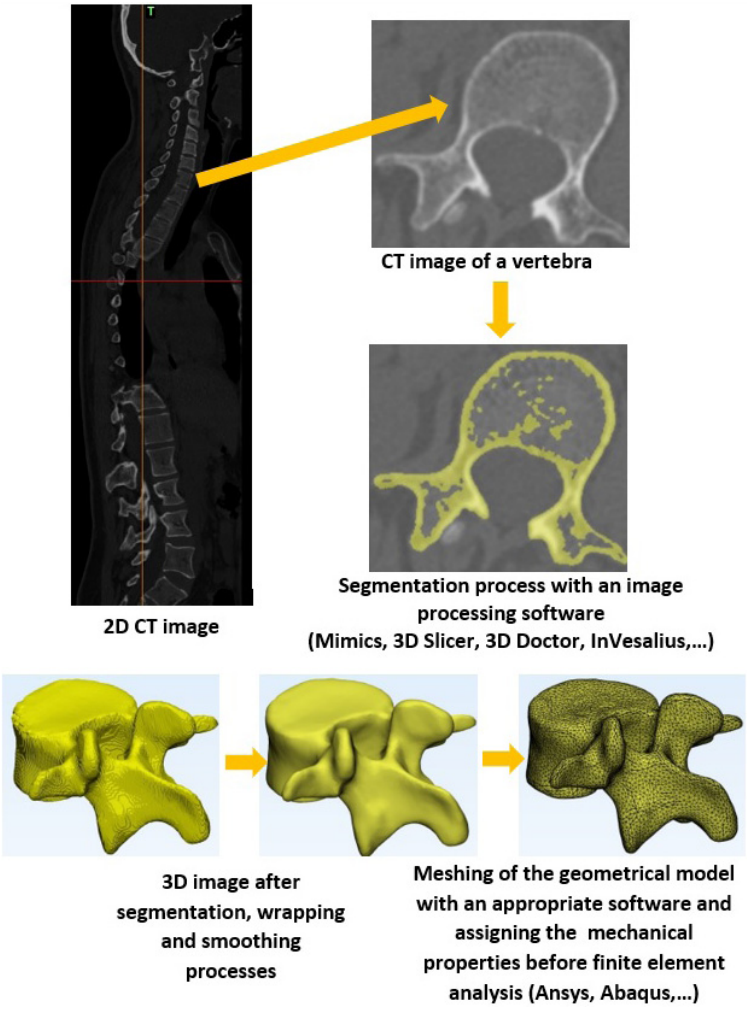

Fig. 7. Flow diagram indicating the steps from the collection of CT images to obtain the finite element model of the human spine.

spine. For this purpose, a suitable image processing software [e.g., Mimics (Materialise's Interactive Medical Image Control System, Belgium), 3D Slicer, 3D Doctor, or Vesalius3D] should be employed to reconstruct the geometry of models from CT images.[22,40] Following CT image processing steps with appropriate segmentation, accurate geometries of spinal bony components can be obtained.[22,35] Also, for the mesh generation, the geometrical model is imported into another software [Abaqus/CAE (Dassault Systémes), Ansys Workbench software (Ansys Inc. Canonsburg, PA, USA), etc.], for FE analysis.[28]

Several research groups have been studying to improve fast and accurate modeling procedures for orthopedic structures. Huang *et al.* modified the

conventional approach to enhance software operating procedures. In their study, CT images of different bone tissues were used for the reconstruction of models. This procedure involves image segmentation, an arrangement of the edge length and meshes, and also the assignment of material properties that are related to the corresponding gray values.[35]

In addition to this method, also MRI can be used to obtain the structural geometry. MRI scans allow users to determine the structures that cannot be seen from CT scans.[22]

In the modeling process, it is necessary to have CT images in the file format of DICOM. After transferring the scan data, modeling software is needed to convert the DICOM data to images in different anatomical planes (horizontal, coronal, and sagittal planes). First of all, a computer-aided design (CAD) or solid model is constructed, then the meshing process is performed with different methods (Fig. 8). Generally, a mixture of the tetrahedral, wedge, and hexahedral elements has been used for the generation of FE models.[41] Following this meshing section, musculoskeletal models can be employed for the FE analysis.[35]

To reconstruct the bone structure, HU threshold values can be used in modeling software.[42] HUs are dimensionless variables used in CT imaging to indicate CT numbers in a standardized form. Different tissues of the body are represented by appropriate HU values depending on their densities in the grayscale level. For instance, a HU value of −1000 is for air, 0 HU for water, and +1000 HU for bone density.[43] CT data has been employed for measuring the HU values to evaluate the

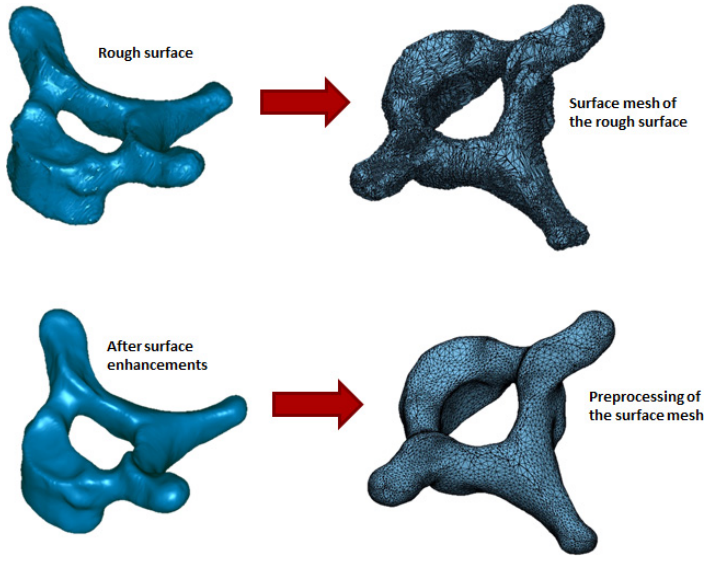

Fig. 8. Surface processing of a vertebra indicating the improvement of surface mesh. After enhancements, an ideal surface mesh is obtained.

vertebral bone quality, which is related to mineral density and strength of the bone.[43,44]

To assign the mechanical properties to the bone segments, HU values can be used. HU value for the cancellous bone is associated between 200 and 500 and the apparent density is between 0.75 and 0.97 g/cm^3.[45] According to Yosibash *et al.*, the HU value for the cortical bone is higher than 700 (HU > 700) and less than 700 for the cancellous bone.[46]

The relationship between the HU value and bone density (ρ) can be constructed by using the following equation (Eq. (1)):

$$\rho = 1.122 \times \mathrm{HU} + 47. \tag{1}$$

Although only one elastic modulus value was assigned to specify the mechanical properties of the bone tissue in some studies (i.e., elastic modulus = $0.63 \times \rho^{1.35}$ MPa),[47,48] two different bone segments should be considered for a more realistic FE model. To have the distinction between the cortical and cancellous bones, the following equations (Eqs. (2) and (3)) can be used[45]

$$E_{\text{cancellous}} = 1.904 \times \rho^{1.64}, \tag{2}$$

$$E_{\text{cortical}} = 2.65 \times \rho^{3.09}. \tag{3}$$

Figure 9 represents the vertebra after material assignment. Firstly, the 3D solid vertebra model is created, the volumetric mesh is completed then to indicate

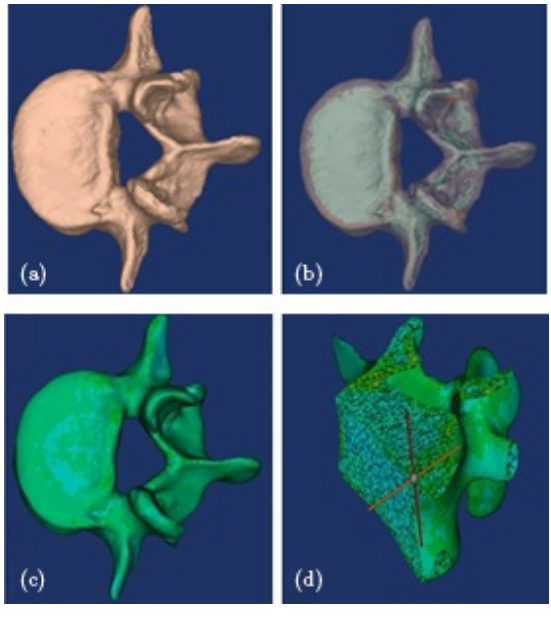

Fig. 9. (a) 3D model of the L4 vertebra, (b) inner side of the vertebra that is composed of cancellous and trabecular parts, and (c) and (d) material properties that were assigned before finite element analysis.

the number of material densities in this part, and finally, material assignment (elastic modulus and Poisson's ratio) can be applied to the remeshed object.

4. Element Types Used for Spinal Components

Various element types and structures have been used in FE modeling of the spine. Table 1 summarizes different types of elements that have been used in the literature for the vertebrae, intervertebral discs, facet joints, and ligaments.

4.1. *Modeling of the vertebrae*

In the modeling process, the vertebral bodies and posterior elements can be constructed separately. In the segmentation stage, posterior elements and vertebral bodies can be split into two parts by deleting rows of pixels in different plane regions. Following this separation, posterior parts may also be divided into different segments to create much simpler geometries. Thus, several segmentation masks can be used for the modeling.[28]

The vertebrae consist of the cortical and cancellous bones and posterior structures. To simulate the cortical bone around the cancellous, a shell element can be used.[5,11,49–51] Figure 10 represents the segmentation procedure of a vertebral body. The green region (obtained with the green mask) is the trabecular (or cancellous) bone and the blue region (obtained with the blue mask) that surrounds the trabecular bone indicates the cortical bone.

4.2. *Modeling of the intervertebral discs and facet joints*

Excessive deformation and degeneration of the intervertebral discs are the main cause of the pathologies in the spinal column. These disc structures, which are located between each pair of vertebrae, are soft tissues.[56,59,60]

In many spinal diseases including lumbar spinal disease and degenerative scoliosis, the modeling of the intervertebral disc and also the facet joints have been constructed with various types of elements and materials. They have been created with different approaches.[4,5,30,58,59] Since these spinal structures are not seen in CT scans, one of these methods is manual segmentation. In this technique, the CT image is used to develop the spinal components with different segmentation masks.[40] Figure 11 shows an example of manual segmentation. Various segmentation masks with different colors indicate the inner layers of the intervertebral discs between the adjacent vertebrae. After this process, 3D solid structures could be obtained.

Besides the manual segmentation of CT scans, the intervertebral disc structure can be developed by the "loft" option in CAD software such as SolidWorks (Dassault Systemes, MA, USA) or a similar 3D CAD design software. The lofted structure is developed between the two parallel surfaces, namely, between the lower side of one vertebra and the upper side of the other vertebrae. An example of the final version of a disc structure is seen in Fig. 12. After obtaining the full disc structure, the nucleus

Table 1. Element types and material properties assigned to finite element models of the spinal structures.

Spinal structure	Element type	Modulus of elasticity (E) (MPa)	Poisson's ratio	The thickness of the cross-sectional area (mm^2)
Cortical bone	Six-node points triangular facet shell element[5] Hexahedral element[49] Four-node shell[50] Volumic (solid)[51] Shell element[52]	11300[50] 10000[49] 12000[5,51–55]	0.2[50] 0.3[5,49,51–55]	
Cancellous bone	10-node points tetrahedron solid element[5] Tetrahedral element[54] Hexahedral element[49] Eight-node brick element[50] Volumic (solid)[51] Tetrahedral element[52]	140[50] 100[5,51–54] 450[49]	0.2[50–54] 0.3[5] 0.25[49]	
Lamina terminalis	10-node points tetrahedron solid element[5]	4000[5]	0.4[5]	
Ground mass of the annulus fibrosus (disc annulus)	10-node points tetrahedron solid element[5] Hexahedral, eight-nodes (hyperelastic, incompressible)[56] Hexahedral element[50,54]	4.2[5,49,51,53,54]	0.45[5,49,51,53,54]	
Annulus (fiber)	Two-node points cord element[5] Rebar[49] Eight-node brick[50]	450[49] Hyperelastic, Mooney–Rivlin ($C_{10} = 0.7$, $C_{01} = 0.2$)[50]	0.3[49]	
Nucleus pulposus	10-node points tetrahedron solid element[5] Hexahedral element (incompressible fluid)[54] Incompressible fluid element[49] Four-node hydrostatic fluid (incompressible)[50] Eight-noded brick[28] Eight-noded brick element (isotropic, elastic)[57]	4[5] 1[28,49,53–55] 2[57]	0.49[5,54] 0.499[28,49,53,55,57]	

Table 1. (*Continued*)

Spinal structure	Element type	Modulus of elasticity (E) (MPa)	Poisson's ratio	The thickness of the cross-sectional area (mm^2)
Articular cartilage	10-node points tetrahedron solid element[5]	1000[5]	0.3[5]	
Contact face of the superior articular process	Six-node points triangular facet object element[5]			
Contact face of the inferior articular process	Six-node points triangular object shell element[5]			
Anterior longitudinal ligament (ALL)	Tension only, truss elements two-node spring[49] Two-node points cord element[5] Two-node spring element[50]	15 (< 12%), 30 (> 12%)[49] piecewise, nonlinear elastic[50] 7.8 (< 12%), 20 (> 12%)[53] 20[54] 7.8[58]	0.3[49,53,58] 0.4[54]	11.1[49] 75.9[5] 66[58]
Posterior longitudinal ligament (PLL)	Two-node points cord element[5] Tension only, truss elements[49] Two-node spring element[50]	10 (< 12%), 20 (> 12%)[49] 20[54] Piecewise, nonlinear elastic[50] 10 (< 11%), 20 (> 11%)[53] 10[58]	0.3[49,53,58] 0.4[54]	51.8[5] 11.3[49] 26[58]
Ligamentum flavum (LF)	Two-node points cord element[5] Tension only, truss elements[49]	15.0 (< 6.2%), 19.5 (> 6.2%)[53] 5 (< 25%), 10 (> 25%)[49]	0.3[49,53]	46[49] 78.7[5]
Capsular ligament (CL)	Two-node points cord element[5] Tension only, truss elements[49] Tension only, truss elements (hypoelastic)[57]	7 (< 30%), 30 (> 12%)[49] 7.5 (< 25%), 32.9 (> 25%)[53] 10[54] 7.5 (< 25%), 32.9 (> 25%)[57]	0.3[49,53,54,57]	102.5[5] 42.2[49]
Intertransverse ligament (ITL)	Two-node points cord element[5] 10 (< 18%), 58.7 (> 18%)[53] Truss element[22]	10[58] 10.0 (< 18%), 58.7 (> 18%)[22] 10[59]	0.3[22,58]	40.5[5] 2[58] 0.3[59]

Table 1. (*Continued*)

Spinal structure	Element type	Modulus of elasticity (E) (MPa)	Poisson's ratio	The thickness of the cross-sectional area (mm^2)
Supraspinuos ligament (SSL)	Two-node points cord element[5] Tension only, truss elements[49] Tension only, spring elements[54]	8.0 (< 20%), 15.0 (> 20%)[53] 4 (< 20–40%), 8 (> 40%)[49] 8[58]	0.3[49,53,58]	75.7[5] 13[49] 30[58]
Cartilage endplate	Hexahedral element[49] Shell element[52]	12000[53] 3500[49] 1000[52]	0.3[52,53] 0.25[49] 0.4[55]	
Posterior bone	Ten-node link elements (tension resistance only)[53]	3500[53]	0.25[53]	
Facet (apophyseal) joint	Contact (GAP) element[28,51] Nonlinear soft contact, GAPUNI[49] Shell element[52]	75[52] 23.8[55]	0.4[52,55]	

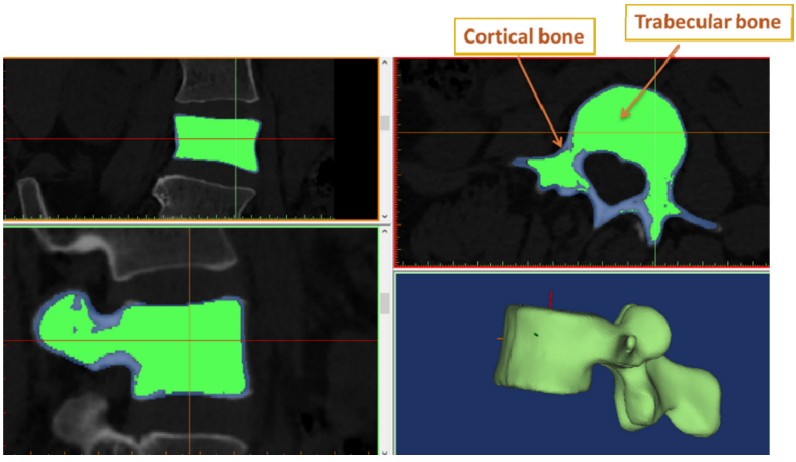

Fig. 10. Representation of the segmentation of a vertebral body with the cortical and trabecular regions.

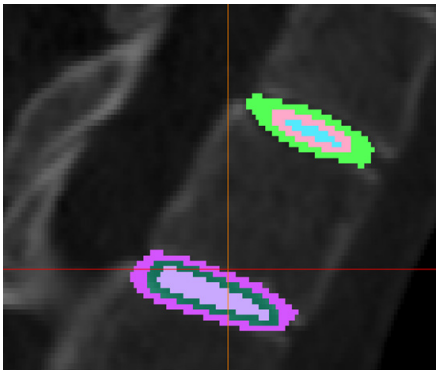

Fig. 11. Manual segmentation of the intervertebral discs in a CT image with different segmentation masks indicating the inner layers of the discs.

pulposus and annulus fibrosus sections can also be developed, along with the appropriate anatomical features in the spine.

The nucleus pulposus can be modeled as an incompressible viscoelastic liquid.[61,62] The collagen fibers are positioned with an angle of $\pm 30^{\circ}$ in the groundmass of the annulus fibrosus.[63] In addition, the collagen fibers can also be modeled with tension resistance.[18]

Another manual creation method can be applied between the adjacent endplates for the construction of the intervertebral discs. For the meshing of these structures, radial displacement of nodes could be employed to assign annulus fibers into the intervertebral discs. The circular mesh pattern is employed for the intervertebral disc to model the concentric rings of the annulus region. The annulus fibers that are oriented at $\pm 30^{\circ}$ can be restricted only under tension loading.[18] For modeling of the

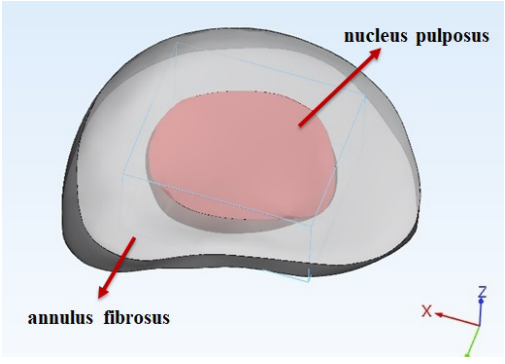

(a)

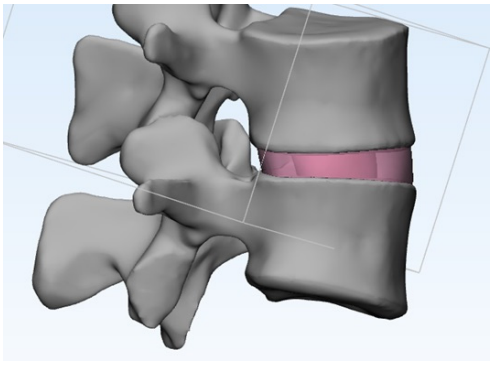

(b)

Fig. 12. (a) Construction of the nucleus and annulus fibrosus of an intervertebral disc and (b) representation of the disc structure in a functional spinal unit.

annulus fibers, the rebar element can be optionally employed. Also, to imitate the collagen fibers, the truss element can be used.[63]

Bredbenner *et al.* defined intervertebral discs as surface node sets that were constructed onto the approximate regions on both superior and inferior vertebrae in the cervical spine model, outlining the boundaries of the intervertebral disc.[64] To get a closed surface along the endplate surfaces, splines were constructed and fit for each of the surfaces on adjacent endplates. In addition, the annulus fibrosus region was modeled with hexahedral elements and was considered to consist of three main regions including anterior, posterior, and lateral parts. The nucleus pulposus of the intervertebral disc was constructed with a fluid-filled membrane element. Anisotropic hyperelastic properties are used to represent the regions of the annulus fibrosus.[64]

Unlike intervertebral discs, facet joints can be represented as rigid structures. They can also be developed by manual segmentation. Figure 13 represents the facet joint development through the adjacent vertebrae with the fascia mask.

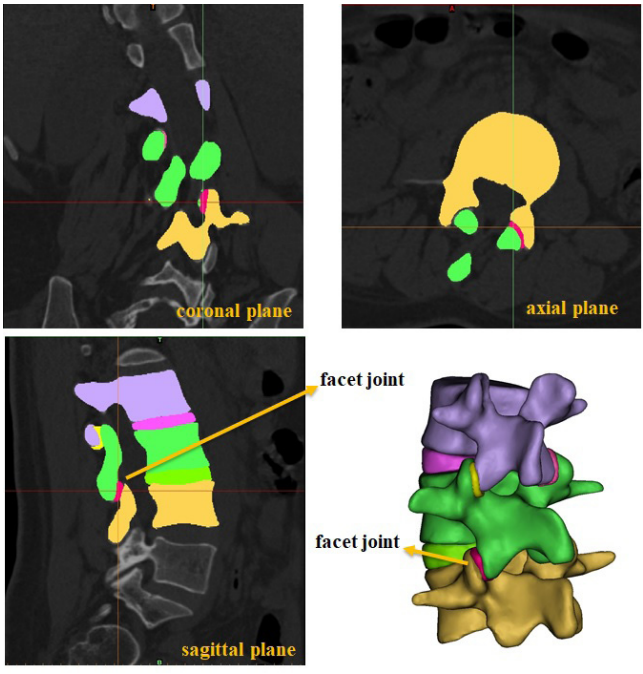

Fig. 13. Intervertebral discs and facet joints obtained after manual segmentation.

Similar to the other spinal components, various element types have been used for facet joints. For instance, in a study, the facet joint cartilage was represented by facet surfaces that were projected as surface triangles throughout the vertex normal.[64] To increase the maximum joint contact without any interference with the facet surface, a constant thickness value was used for each of the facet cartilage elements. As well as ligaments, the facet joint capsules were also represented with discrete spring elements in the models for the connection with the adjacent vertebrae.[64]

Additionally, interface gap elements (ABAQUS element type GAPUNI) can also be used for modeling the facet joints to simulate the contact between the articulating facets.[28] The elements can be employed in the modeling process in two ways; the nodes of the model can be connected as a gap close or the nodes can be separated as an open gap in the modeling process.[65]

According to CT scan measurements, the faces have both convex and concave sides.[22,28] Three layers of hex elements were also used in another study for the representation of facet cartilages with a gap of 0.1 mm.[66] During the simulation processes, the contact behavior of the facet articular surfaces was considered frictionless.[4,30,59,66,67] For the cartilage formation, a 0.6 mm mesh was used to represent the facet joints. A surface-to-surface contact element with a friction coefficient of 0.1 was used in a study.[54] In a different study, with the same element type and friction

coefficient, facet joints were constructed as nonlinear 3D contact pairs to treat their sliding behavior between vertebrae,[11] since facet joints are considered that they could transmit compressive forces with the same rigidity to the surrounding bones.[59,60]

4.3. *Modeling of the ligaments*

The anatomical regions of the ligaments should be accurately selected for the correct arrangement. The seven load-bearing soft tissues (the anterior and posterior longitudinal ligament (ALL, PLL), supraspinous and interspinous ligament (SSL, ISL), intertransverse ligament (ITL), facet capsular ligament (FCL), and ligamentum flavum (LFL)) passing through each functional spinal unit can be represented by two-noded 3D nonlinear elements.[14] Also, different elements can be employed for these structures such as two-node 3D truss elements.[63]

Ligaments could also be simulated with cord elements,[5] 10-node link elements,[53] or tension-only spring elements with nonlinear elastic properties where the materials are linear and homogeneous.[54]

Discrete spring elements were also used in several studies for FE modeling of the ligaments.[64,66] These spring structures allowed the connection of the nodes onto the adjacent vertebrae throughout the spine. The attachment regions on the vertebrae are set after the meshing process.

In an important study, Chazal *et al.* reported some biomechanical properties of 43 human spinal ligaments obtained from fresh cadavers and living subjects.[14] Based on this study, we represented the cross-sectional areas and lengths of the ligaments of the spine in Table 2. According to this valuable information,[14] accurate anatomical segmentation of ligaments can be performed.

Figure 14 indicates the manual segmentation in modeling of the ligaments (anterior, posterior, and interspinous ligaments and ligamentum flavum) in axial and sagittal planes. Following this stage, the segmented regions are obtained as 3D parts.

4.4. *Modeling of spinal implants*

In recent years, as a result of the developments of material properties in spinal instrumentation, deformity correction interventions have been progressively improved.[18,53–55,63,68,69]

In the treatment of spinal injuries, various spinal implants have been used for different purposes. For example, pedicle screws and rods with an intervertebral cage can be employed for posterior fusion operations to provide stability.[69] The rigid rods in the pedicular instrumentation can be made of stainless steel or titanium. At the surgical treatment, screws and rods together increase the fusion rate.[55] In addition, dynamic fixation systems can also be used. Pedicle screw-based dynamic fixation systems have been employed in various studies.[68] This implant system has been employed both for dynamic fixation purposes to maintain the joint motion and also used as an adjunct for fusion operations.[68]

Table 2. Cross-sectional areas and lengths of ligaments in the spine.[14]

	Level	Cross-sectional area (mm^2)	Length (mm)
Anterior longitudinal ligament	C3–C4	13	6
	T4–T5	36	5
	T6–T7	30	6
	T10–T11	25	7
	L1–L2	44	11
	L3–L4	70	13
	L3–L4	74	12.5
	L4–L5	74	12.5
	L4–L5	66	12.5
Posterior longitudinal ligament	C2–C3	10	4.5
	C7–T1	11	5
	C7–T1	9	6
	T4–T5	17	6
	T12–L1	19	9.5
	L1–L2	20	11.5
	L2–L3	34	12.5
	L2–L3	26	10.5
	L2–L3	21	10.5
	L3–L4	19	12.5
Ligamentum flavum	T4–T5	34	12.5
	T5–T6	26	11.5
	T6–T7	29	13
	T7–T8	25	13
	T8–T9	19	13
	T10–T11	30	12
	L3–L4	39	19
Supra and interspinal ligament	T1–T2	9	12
	T2–T3	8	10.5
	T4–T5	8	10
	T7–T8	30	11
	T8–T9	29	10
	L3–L4	29	8
	L3–L4	34	12
	L4–L5	47	11.5
	L4–L5	55	9
	L4–L5	36	10
	L4–L5	24	12
	L4–L5	11	13
	L5–S1	26	11.5
	L5–S1	11	14
Intertransverse ligaments	T7–T8	1.7	8.5
	T9–10	2	9

In Fig. 15(a), the CT image of the L2 vertebra before the surgical operation is seen. The insertion of the screws through the pedicles is given in Fig. 15(b) and the geometrical structure of the screws is represented in Fig. 15(c).

Table 3 shows several implant types and their material properties in the literature.

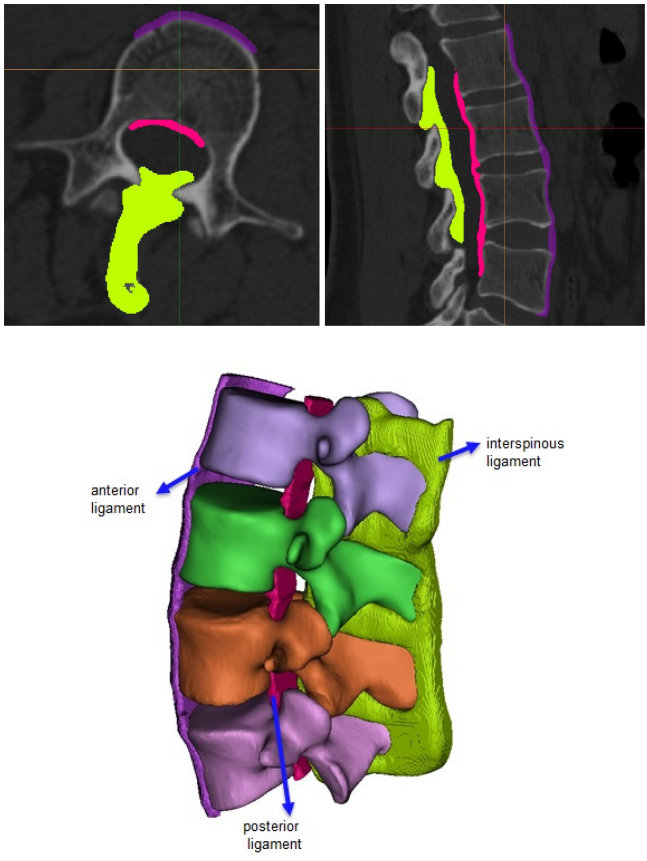

Fig. 14. Segmentation of the ligaments (anterior, posterior, and interspinous ligaments) from CT scans in axial and sagittal planes, and the 3D view of the L2–L5 with the corresponding ligaments.

It is critical to determine the load distribution over the human vertebral column during different activities, especially in the patients subjected to spinal implantation surgeries due to scoliosis. In addition, as a result of the determination of the load distribution via 3D FE analysis, an appropriate posture of the trunk can be

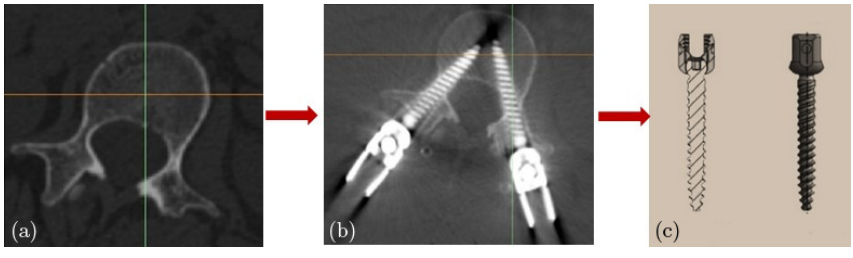

Fig. 15. CT image of the L2 vertebra (a) from pre-operation and (b) post-operation stages and (c) spinal pedicle screws that are inserted into in the surgery.

Table 3. Implant types and material properties.

Research group	Implants properties	Modulus of elasticity (MPa)	Poisson's ratio	Implant materials
Zahaf *et al.*[53]	Pedicle screws	Metal sections 112,400 (the Model B Dyne)	Metal sections 0.34 (the Model B Dyne)	Metal sections titanium with elastic properties Deformable sections (elastic material-silicone)
		Deformable Sections 600 (the Model B Dyne)	deformable sections 0.49 (the Model B Dyne)	
	Metal parts and deformable rods pedicle (Elaspine implant)	113,000 (pedicle screw)	0.3 (pedicle screw)	Metal parts (titanium alloy), deformable rods (polymer)
		(deformable sections) 600	(deformable sections) 0.49	
	Bioflex implant	113,000	0.3	Titanium alloy
	Cofflex rivet model	113,000	0.3	Titanium alloy
	Pedicle screw	113,000	0.3	Titanium alloy (fixation at the lumbar segment)
Gong *et al.*[54]	Transforaminal lumbar interbody fusion (TLIF)	145,000	0.3	Titanium
Abe *et al.*[63]	Simultaneous double-rod rotation technique (SDRRT)	105,000 (yield stress 900, yield strain 8.57×10^{-3}, hardening coefficient: 2.41 GPa)		Titanium rod
Galbusera *et al.*[55]	pedicular screws	110,000	0.3	
	Rods	210,000	0.3	Stainless steel
	Rods	110,000	0.3	Titanium
	Rods	3500	0.3	PEEK
Lv *et al.*[52]	Interbody cage	4340	0.4	PEEK, tetrahedral element
	Screw	110,000	0.3	Titanium, tetrahedral element

Table 3. (*Continued*)

Research group	Implants properties	Modulus of elasticity (MPa)	Poisson's ratio	Implant materials
Little *et al.*[50]	Screws	108,000	0.3	Linear elastic, titanium alloy
	Rods	108,000	0.3 (yield stress = 390 MPa)	Linear elastic, perfectly plastic
Nemade *et al.*[70]	Pedicle screws and tightening screws	110,000	0.3 (density $= 4.43\text{E}-09\,\text{tones/mm}^3$)	Linear elastic and isotropic
	Rods	110,000	0.3	Linear elastic and isotropic
Xu *et al.*[71]	Pedicle screws	114,000	0.3	Homogeneous and isotropic materials
Kim *et al.*[72]	Pedicle screws	110,000	0.3	Titanium alloy (20-node solid element)
	Spinal rod	110,000	0.3	Titanium alloy (20-node solid element)

determined, thereby leading the researchers to prevent and evaluate the spinal disorders effectively.[63]

The pedicle screw fixation system consists of rods and pedicle screws. To represent the pedicle screws, cylinders can be used. Also, the interface between the screw and the bone can be assigned to be fully constrained. The pedicle screw fixation system maintains the structure of supraspinous ligaments and interspinous ligaments. The pedicle screws are inserted through the pedicles of the vertebrae bilaterally.[53]

In the study of Chen *et al.*, the approach for creating a screw trajectory is explained step-by-step.[42] Firstly, they created a cylinder using the MEDCAD module in Mimics software (Materialise's Interactive Medical Image Control System, Belgium). They decided on the starting and ending points of the screw trajectory. The simulation of the screw trajectory is adjusted in each plane (sagittal, coronal, and axial) or 3D reconstructed object. After setting up the position of the screw trajectory, the 3D model of the screw trajectory could be obtained. The radius, color, length, and also preoperation angle of the simulated object could be adjusted at this point for further studies.[42]

5. Conclusion

This paper provides a detailed review of the FE spine models and the spinal research. A wide range of modeling techniques has been introduced throughout the study. The anatomical features of the spine and the spinal components have been briefly explained. Besides, the development of the finite element spine models has been introduced including all the components of the spine including vertebrae, various ligaments, facet joints, and intervertebral discs. We emphasized that the modeling stages of the spine and the corresponding structures, and also the design of the spinal instruments as a finite element model, are crucial to obtain the correct FE models. In order to correctly evaluate the biomechanical behavior of the spine under different loading and boundary conditions, an accurate computational model should be inevitably constructed. We expect that this study will provide a complementary perspective to researchers studying spinal biomechanics.

Acknowledgments

The authors declare no conflict of interest.

References

1. Panjabi MM, White AA, *Clinical Biomechanics of Spine*, Lippincott Williams & Wilkins, 1990.
2. Boos N, Aebi M, *Spinal Disorders: Fundamentals of Diagnosis and Treatment*, Springer, 2008.
3. Kurtz SM, Edidin AA, *Spine Technology Handbook*, Elsevier Academic Press, 2006.
4. Wang L, Zhang B, Chen S, Lu X, Li ZY, Guo Q, A validated finite element analysis of facet joint stress in degenerative lumbar scoliosis, *World Neurosurg* **95**:126–133, 2016.

5. Zheng J, Yang Y, Lou S, Zhang D, Liao S, Construction and validation of a three-dimensional finite element model of degenerative scoliosis, *J Orthop Surg Res* **10**(1):1–7, 2015.
6. Oxland TR, Fundamental biomechanics of the spine — What have we learned in the past 25 years and future directions, *J Biomech* **49**(6):817–832, 2015.
7. Bashkuev M, Reitmaier S, Schmidt H, Relationship between intervertebral disc and facet joint degeneration: A probabilistic finite element model study, *J Biomech* **102**:1–30, 2020.
8. Erdemir A, Guess TM, Halloran J, Tadepalli SC, Morrison TM, Considerations for reporting finite element analysis studies in biomechanics, *J Biomech* **45**:625–633, 2012.
9. Kotwal S, Pumberger M, Hughes A, Girardi F, Degenerative scoliosis: A review, *Hosp Spec Surg J* **7**:257–264, 2011.
10. Li J, Xiao H, Zhu Q, Li C, Liu H, Huang Z, Shang J, Novel pedicle screw and plate system provides superior stability in unilateral fixation for minimally invasive transforaminal lumbar interbody fusion: An *in vitro* biomechanical study, *PLoS One* **10**(3):1–13, 2015.
11. Coombs DJ, Laz PJ, Rao M, Smith SD, Bushelow M, Rullkoetter PJ, Stepwise validated finite element model of the human lumbar spine, *Simulia Cust Conf* **2012**:1–15, 2012.
12. Wilke HJ, Herkommer A, Werner K, Liebsch C, *In vitro* analysis of the segmental flexibility of the thoracic spine, *PLoS One* **12**(5):1–16, 2017.
13. Zwambag DP, Brown SHM, Experimental validation of a novel spine model demonstrates the large contribution of passive muscle to the flexion relaxation phenomenon, *J Biomech* **102**:109431, 2020.
14. Chazal J, Tanguy A, Bourges M, Gaurel G, Escande G, Guillot M, Vanneuville G, Biomechanical properties of spinal ligaments and a historical study of the supraspinal ligament in traction, *J Biomech* **18**(3):167–176, 1985.
15. Frost HM, An approach to estimating bone and joint loads and muscle strength in living subjects and skeletal remains, *Am J Hum Biol* **11**(4):437–455, 1999.
16. Shojaei I, Hendershot BD, Acasio JC, Dearth CL, Ballard M, Bazrgari B, Trunk muscle forces and spinal loads in persons with unilateral transfemoral amputation during sit-to-stand and stand-to-sit activities, *Clin Biomech* **63**:95–103, 2019.
17. Fagan MJ, Julian S, Mohsen AM, Finite element analysis in spine research, *Proc Ins Mech Eng H: J Eng Med* **216**(5):281–298, 2002.
18. Shiraz-Adl A, El-Rich M, Pop DG, Parnianpour M, Spinal muscle forces, internal loads and stability in standing under various postures and loads-application of kinematics-based algorithm, *Eur Spine J* **14**(4):381–392, 2005.
19. Kikkawa J, Cunningham BW, Shirado O, Hu N, McAffee PC, Oda H, Biomechanical evaluation of a posterolateral lumbar disc arthroplasty device-an *in vitro* human cadaveric model, *Spine* **35**(19):1760–1768, 2010.
20. Barbera LL, Wilke HJ, Liebsch C, Villa T, Luca A, Galbusera F, Brayda-Bruno M, Biomechanical *in vitro* comparison between anterior column realignment and pedicle subtraction osteotomy for severe sagittal imbalance correction, *Eur Spine J* **29**(1):36–44, 2020.
21. Zhou C, Cha T, Li G, An upper bound computational model for investigation of fusion effects on adjacent segment biomechanics of the lumbar spine, *Comput Method Biomech Biomech Eng* **22**(14):1126–1134, 2019.
22. Hassan CR, Finite element model development of the human lumbar spine and dynamic stabilization device analysis, MS. Thesis, Koç University, 2015.
23. Sullivan TB, Reighard FG, Osborn EJ, Parvaresh KC, Newton PO, Thoracic idiopathic scoliosis severity is highly correlated with 3D measures of thoracic kyphosis, *J Bone Joint Surg* **99**(11):e54, 2017.

24. Janicki JA, Alman B, Scoliosis: Review of diagnosis and treatment, *Paediatr Child Health* **12**(9):771–776, 2007.
25. Subach BR, Martin MM, Copay AG, Califano CB, Claassen LB, Bologna LA, Spines in motion: Biomechanics of the spine, *J Spinal Res Found* **7**(2):1–64, 2012.
26. Nouh MR, Spinal fusion-hardware construct: Basic concepts and imaging review, *World J Radiol* **4**(5):193, 2012.
27. VanPutte C, Regan J, Russo A, *Seeley's Essentials of Anatomy & Physiology*, McGraw-Hill Education, 2016.
28. Tyndyk MA, Barron V, McHugh PE, O'Mahoney D, Generation of a finite element model of the thoracolumbar spine, *Acta Bioeng Biomech* **9**(1):35–46, 2007.
29. Schmidt H, Galbusera F, Rohlmann A, Shirazi-Adl A, What have we learned from finite element model studies of lumbar intervertebral discs in the past four decades?, *J Biomech* **46**(14):2342–2355, 2013.
30. Jaumard NV, Welch WC, Winkelstein BA, Spinal facet joint biomechanics and mechanotransduction in normal, injury and degenerative conditions, *J Biomech Eng* **133**(7):071010, 2011.
31. Rao M, Explicit finite element modelling of the human lumbar spine, Ph.D. Thesis, University of Denver, 2010.
32. Myklebust JB, Pintar F, Yoganandan N, Cusick JF, Maiman D, Myers TJ, Sances A, Tensile strength of spinal ligaments, *Spine* **13**(5):526–531, 1988.
33. Hines T, Functional anatomy of the spine, *Mayfield Clin-Brain & Spine* 1–5, 2016.
34. Celenk C, Celenk P, *Bone Density Measurement Using Computed Tomography, Computed Tomography-Clinical Applications*, Springer, Berlin, pp. 123–136, 2012.
35. Huang H, Xiang C, Zeng C, Ouyang H, Wong KKL, Huang W, Patient-specific geometrical modeling of orthopedic structures with high efficiency and accuracy for finite element modeling and 3D printing, *Aust Phys Eng Sci Med* **38**(4):743–753, 2015.
36. Chen C, Ruan D, Wu C, Wu W, Sun P, Zhang Y, Wu J, Lu S, Ouyang J, CT morphometric analysis to determine the anatomical basis for the use of transpedicular screws during reconstruction and fixations of anterior cervical vertebrae, *PLoS One* **8**(12):1–10, 2013.
37. Hotchkiss WR, Schwend RM, Bosch PP, Edgar HJH, Young BN, Defining the differences in transverse plane trajectories for thoracic pedicle screw insertion: anatomic versus medial, *Spine Deform* **4**(1):22–26, 2016.
38. Hu X, Siemionow KB, Lieberman IH, Thoracic and lumbar vertebrae morphology in lenke type 1 female adolescent idiopathic scoliosis patients, *Int J Spine Surg* **8**(30):1–12, 2014.
39. Yoo JU, Ghanayem A, Petersilge C, Lewin J, Accuracy of using computed tomography to identify pedicle screw placement in cadaveric human lumbar spine, *Spine* **22**(22):2668–2671, 1997.
40. Faria SP, Biomechanical analysis of the human lumbar spine-an experimental and computational approach, MS. Thesis, Technical University of Lisbon, 2015.
41. Kim YH, Khuyagbaatar B, Kim K, Recent advances in finite element modeling of the human cervical spine, *J Mech Sci Technol* **32**(1):1–10, 2018.
42. Chen D, Chen CH, Tang L, Wang K, Li YZ, Phan K, Wu AM, Three-dimensional reconstructions in spine and screw trajectory simulation on 3D digital images: a step-by-step approach by using mimics software, *J Spine Surg* **3**(4):650–656, 2017.
43. Silva IMCC, Freitas DQ, Ambrosano GMB, Boscolo FN, Almeida SM, Bone density: comparative evaluation of Hounsfield units in multislice and cone-beam computed tomography, *Braz Oral Res* **26**(6):550–556, 2012.

44. Schreiber JJ, Hughes AP, Taher F, Girardi FP, An association can be found between Hounsfield units and success of lumbar spine fusion, *Hosp Spec Surg J* **10**(1):25–29, 2014.
45. Dogru SC, Cansız E, Arslan YZ, A review of finite element applications in oral and maxillofacial biomechanics, *J Mech Med Biol* **18**(2):1–26, 2018.
46. Yosibash Z, Trabelsi N, Milgrom C, Reliable simulations of the human proximal femur by high-order finite element analysis validated by experimental observations, *J Biomech* **40**(16):3688–3699, 2007.
47. Aparna CS, Tewari RP, Govil AK, Biomechanical analysis of a three-dimensional finite element model, *Int J Theor Appl Res Mech Eng* **2**(2):155–158, 2013.
48. Moon YL, Jung S, Park SH, Choi GY, Evaluation of focal bone mineral density using three-dimensional measurement of Hounsfield units in the proximal humerus, *Clin Shoulder Elbow* **18**(2):86–90, 2015.
49. Zafarparandeh I, Erbulut DU, Ozer AF, Influence of three-dimensional reconstruction method for building a model of the cervical spine on its biomechanical responses: A finite element analysis study, *Adv Mech Eng* **8**(3):1–6, 2016.
50. Little JP, Izatt MT, Labrom RD, Askin GN, Adam CJ, An FE investigation simulating intra-operative corrective forces applied to correct scoliosis deformity, *Scoliosis* **8**(9):1–13, 2013.
51. Ezquerro F, Simon A, Prado M, Perez A, Combination of finite element modeling and optimization for the study of lumbar spine biomechanics considering the 3D thorax-pelvis orientation, *Med Eng Phys* **26**(1):11–22, 2004.
52. Lv QB, Gao X, Pan XX, Jin HM, Lou XT, Li SM, Yan YZ, Wu CC, Lin Y, Ni WF, Wang XY, Wu AM, Biomechanical properties of novel transpedicular transdiscal screw fixation with interbody arthrodesis technique in lumbar spine: A finite element study, *J Orthop Trans* **10**(15):50–58, 2018.
53. Zahaf S, Kebdani S, Biomechanical study between the rigid and dynamic fixation systems of the cpinal column analyzed by the finite element method, *Nano Biomed Eng* **9**(2):167–183, 2017.
54. Gong Z, Chen Z, Feng Z, Cao Y, Jiang C, Jiang X, Finite element analysis of 3 posterior fixation techniques in the lumbar spine, *Orthopedics* **37**(5):441–448, 2014.
55. Galbusera F, Bellini CM, Anasetti F, Ciavarro C, Lovi A, Brayda-Bruno M, Rigid and flexible spinal stabilization devices: A biomechanical comparison, *Med Eng Phys* **33**(4):490–496, 2011.
56. Jaramillo HE, Gomez L, Garcia JJ, A finite element model of the L4-L5-S1 human spine segment including the heterogeneity and anisotropy of the discs, *Acta Bioeng Biomech* **17**(2):15–24, 2015.
57. Shahraki NM, Fatemi A, Goel VK, Agarwal A, On the use of biaxial properties in modeling annulus as a Holzapfel-Gasser-Ogden material, *Front Bioeng Biotechnol* **3**(69):1–9, 2015.
58. Farajpour H, Jamshidi N, Effects of different angles of the traction table on lumbar spine ligaments: A finite element study, *Clin Orthop Surg* **9**(4):480–488, 2017.
59. Xie F, Zhou H, Zhao W, Huang L, A comparative study on the mechanical behavior of intervertebral disc using hyperelastic finite element model, *Technol Health Care* **25**(S1):177–187, 2017.
60. Palepu V, Biomechanical effects of initial occupant seated posture during rear end impact injury, Ph.D. Thesis, The University of Toledo, 2013.
61. Emanuel KS, Veen AJ, Rustenburg CME, Smit TH, Kingma I, Osmosis and viscoelasticity both contribute to time-dependent behaviour of the intervertebral disc under compressive load: a caprine *in vitro* study, *J Biomech* **70**:10–15, 2018.

62. Raheem HM, Bay B, Rochefort S, Viscoelastic properties of a novel hydrogel/foam composites for nucleus pulposus replacement, *Spring Nat Appl Sci* **1**(809):1–9, 2019.
63. Abe Y, Ito M, Abumi K, Sudo H, Salmingo R, Tadano S, Scoliosis corrective force estimation from the implanted rod deformation using 3D-FEM analysis, *Scoliosis* **10**(S2):1–6, 2015.
64. Bredbenner TL, Eliason TD, Francis WL, McFarland JM, Merkle AC, Nicolella DP, Development and validation of a statistical shape modeling-based finite element model of the cervical spine under low-level multiple direction loading conditions, *Front Bioeng Biotechnol* **2**(58):1–12, 2014.
65. Krueger R, Ratcliffe JG, Minguet PJ, Panel stiffener debonding analysis using a shell/3D modeling technique, *Compos Sci Techno* **69**(14):2352–2362, 2009.
66. Du CF, Yang N, Guo JC, Huang YP, Zhang C, Biomechanical response of lumbar facet joints under follower preload: a finite element study, *BMC Musculoskel Disord* **17**(126):1–13, 2016.
67. Campbell JQ, Petrella AJ, An automated method for landmark identification and finite element modeling of the lumbar spine, *IEEE Trans Biomed Eng* **62**(11):2709–2716, 2015.
68. Chen CS, Huang CH, Shih SL, Biomechanical evaluation of a new pedicle screw-based posterior dynamic stabilization device (awesome rod system)- a finite element analysis, *BMC Musculosk Disord* **16**(81):1–8, 2015.
69. Herren C, Beckmann A, Meyer S, Pishnamaz M, Mundt M, Sobottke R, Prescher A, Stoffel M, Markert B, Kobbe P, Pape HC, Eysel P, Siewe J, Biomechanical testing of a PEEK-based dynamic instrumentation device in a lumbar spine model, *Clin Biomech* **44**:67–74, 2017.
70. Nemade A, Shikalgar A, Sancheti S, Wadkar SP, Biomechanical analysis of spinal pedicle screws under static compression and tensile bending, *Mater Today: Proc* **47**:4778–4785, 2021. doi: 10.1016/j.matpr.2021.05.681.
71. Xu M, Yang J, Lieberman IH, Haddas R, Finite element method-based study of pedicle screw–bone connection in pullout test and physiological spinal loads, *Med Eng Phys* **67**:11–21, 2019.
72. Kim CJ, Son SM, Choi SH, Goh TS, Lee JS, Lee CS, Numerical evaluation of spinal stability after posterior spinal fusion with various fixation segments and screw types in patients with osteoporotic thoracolumbar burst fracture using finite element analysis, *Appl Sci* **11**(7):3243, 2021.